Profiling the Beam of the T5 Ion Engine

James E. Pollard
The Aerospace Corporation, P.O. Box 92957, M5-754, Los Angeles, CA 90009

Abstract

Current density profiles in the beam of a xenon ion engine are measured using a long tungsten wire probe to collect ions while making radial traverses through the beam. Between traverses the probe is moved along the axial coordinate to sample the profile at distances of 5-50 cm from the exit plane. Abel inversion of the data provides flux contour maps and integrated current maps as functions of beam voltage and accelerator voltage. Data for the British T5 engine are compared with previous experiments using a thrust balance and an angle-resolving Faraday probe.

Introduction

Studies of the T5 ion thruster in our laboratory have demonstrated the use of angle-resolving Langmuir and Faraday probes, an electrostatic deflection energy analyzer, and a time-of-flight mass and charge analyzer.[1-3] These diagnostics measure the ion flux, electron density, electron characteristic energy, floating potential, plasma potential, ion beam energy, and charge-state distribution as functions of position within the plume. The resulting information on plume properties and discharge chamber erosion is useful for developing mathematical models of life-limiting factors and spacecraft interactions.

Although the basic properties of the T5 plume are now fairly well documented, there are still important questions to be answered. The angle-resolved ion flux exhibits a complex dependence on thrust level and beam energy that is not fully understood.[3] We also would like to determine what fraction of the beam power supply current is due to electrons penetrating the grids and plasma screen rather than to the ejection of high velocity ions. Thrust balance data for the T5 are at least 2%-4% lower than the thrust values derived from the supply current after correcting for divergence and multiply-charged ions.[4] Also suggestive of a thrust loss are angular distributions measured with a Faraday probe that give an integrated beam current about 20% less than the supply current.[3] Finally, we would like to map the ion flux in the region within 50 cm from the exit plane as a function of the voltages applied to the screen and accelerator grids, for comparison with recent Faraday probe data measured further downstream.[5] The experiment described here begins to address these questions by recording beam profiles for the T5 over a wider range of operating points and spatial locations than in previous tests.

Experimental

The test article is a divergent-field xenon ion thruster (10-cm diameter, 3-grid, engineering-model T5 Mk4) developed and manufactured by the UK Defence Evaluation and Research Agency,[6] which for this test is operated at 85% utilization efficiency with performance parameters similar to those given in Reference 3. A distinctive feature of the T5 is that the grids are dished inward to minimize the possibility of a short circuit due to thermal expansion. More than 1000 hours of operation were accumulated on the grid set prior to the present test, including a significant amount of performance mapping at off-nominal operating conditions where the grid erosion rate is enhanced. Corrected background pressure is maintained in the 1.5-2.0 $\times$ 10^{-6} torr range by two re-entrant closed-cycle cryopumps (CVI TM1200) with a combined pumping speed of 7 $\times$ 10^{4} liter/s for xenon. The beam dump consists of carbon-fiber composite plates located 200-240 cm downstream of the thruster exit plane. The beam dump and stainless steel vacuum tank are at ground potential.

Ion currents are measured with a tungsten wire probe (0.099 cm diam $\times$ 32.8 cm long) that is swept through the beam at various distances from the exit plane using a motorized positioning system, as depicted in Fig. 1. The probe moves through the beam along the radial coordinate (x-direction), while the collected current is recorded at 45 locations with increments of 0.635 cm between points. Between each of these radial traverses the probe is moved along the

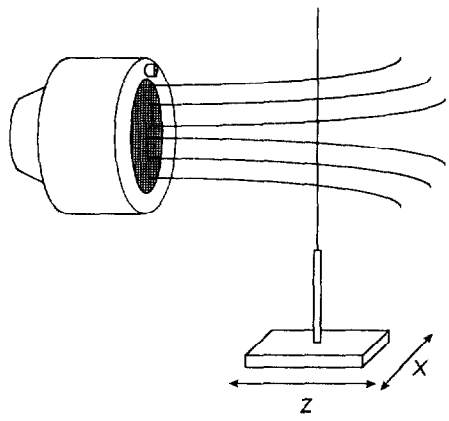

Figure 1. The wire probe makes a radial traverse through the beam along the x-axis while measuring the collected ion current. Between each traverse the probe moves along the z-axis so that the profile is recorded at several distances from the thruster exit plane.

axial coordinate (z-direction) to measure the profile at 6.2, 16.3, 26.5, 36.6, and 46.8 cm from the exit plane. The probe is held at ground potential, and the ion current (typically 1-5 mA) is recorded by a Fluke 45 digital multimeter at 0.001-mA resolution. Sputtered tungsten from the probe is deposited on the front of the thruster and on adjacent surfaces of the test chamber, which is acceptable in the present case, but may argue against applying this diagnostic technique to a flight-model thruster. The decrease in the wire diameter by sputtering was negligible during brief exposure in this test (< 5 hours). One motivation for selecting a long wire probe instead of the short probe used in previous work[1-3] is to obtain a more complete sample of the beam for determining the integrated current. Another advantage is that the probe support tube and insulators are not exposed to the highly erosive ion beam.

Although the flux of high velocity ions is independent of the voltage applied to the probe, the flux of low energy electrons does depend on voltage. With the neutralizer-common and plasma screen tied to the grounded vacuum tank, the neutralizer keeper is 15-20 V positive, and the plasma potential in the beam is 9-12 V positive with respect to ground.[3] Hence when the probe is at ground potential, virtually all of the electrons are repelled (kT_e < 1.5 eV),[1] and the collected current is due primarily to fast ions. Slow charge-exchange ions contribute a small additional current that appears as a non-zero baseline in the periphery of the beam, but this is negligible for the present data sets. The probe wire length (32.8 cm) is chosen to capture the high velocity ions at 5-50 cm from the exit plane while minimizing the contribution from charge-exchange ions. Because the wire diameter D is small

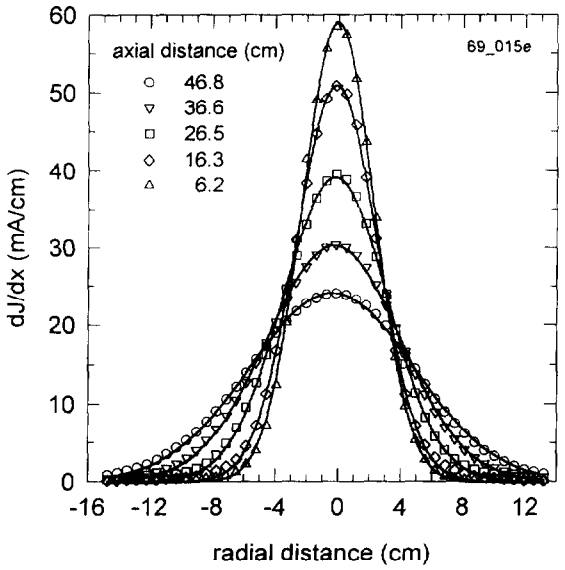

Figure 2. Wire probe data with fitting to Gaussian functions for a beam supply current of 328 mA, beam voltage of 1100 V, and accelerator voltage of –250 V.

compared to the dimensions of the beam, the line-integrated current density dJ/dx can be calculated from the measured probe current J_{probe} by

$$\int_{-\infty}^{\infty} \frac{d^2J}{dx\,dy}\,dy = \frac{dJ}{dx} = \frac{J_{probe}}{D}. \qquad (1)$$

The integral of dJ/dx over all x is J_{total}, which is related to the integrated beam current J_{beam} by

$$\int_{-\infty}^{\infty} \frac{dJ}{dx}\,dx = J_{total} = (1+\eta)\,J_{beam}, \qquad (2)$$

where η is the secondary electron yield, for which an estimate is available ($\eta = 0.04$).[7]

Results

We want to transform the line-integrated current density dJ/dx to the current density in polar coordinates $d^2J/r\,dr\,d\varphi$. Assuming the T5 beam is azimuthally symmetric,[8,9] then dJ/dx is analogous to the line-of-sight radiance $I(x)$ for an axisymmetric plasma or flame, from which the inverse Abel transform gives the radial distribution of emission coefficient $\varepsilon(r)$.[10-14] Reference 14 shows that the inverse Abel transform of a continuous function $I(x)$ is equivalent to a Fourier transform followed by a Hankel transform,

$$G(f) = \int_{-\infty}^{\infty} I(x)\exp(-j\,2\pi f x)\,dx, \qquad (3)$$

$$\varepsilon(r) = 2\pi \int_{0}^{\infty} G(f)\,f\,J_0(2\pi f r)\,df, \qquad (4)$$

where J_0 is the zero-order Bessel function.

Data reduction is facilitated by least-squares fitting of the beam profiles to Gaussian functions. In the example shown in Fig. 2, as in most of the data sets, the profiles are well-represented by

$$\frac{dJ}{dx} = \frac{J_{total}}{\sigma\sqrt{2\pi}}\exp\left[-\frac{1}{2}\left(\frac{x-x_0}{\sigma}\right)^2\right], \qquad (5)$$

where the fitting parameters are J_{total}, x_0, and σ. We are only interested in J_{total} and in the width parameter σ, because x_0 is simply the zero offset of the probe positioning system. At a few of the thruster operating points, Eq. (5) is a less-than-perfect representation of the data, but we have not thus far attempted to improve on it. Three advantages of this approach to fitting the data are that the zero offset x_0 is easily determined, that the data can be readily extrapolated beyond the range of measurement, and that an inverse Abel transform

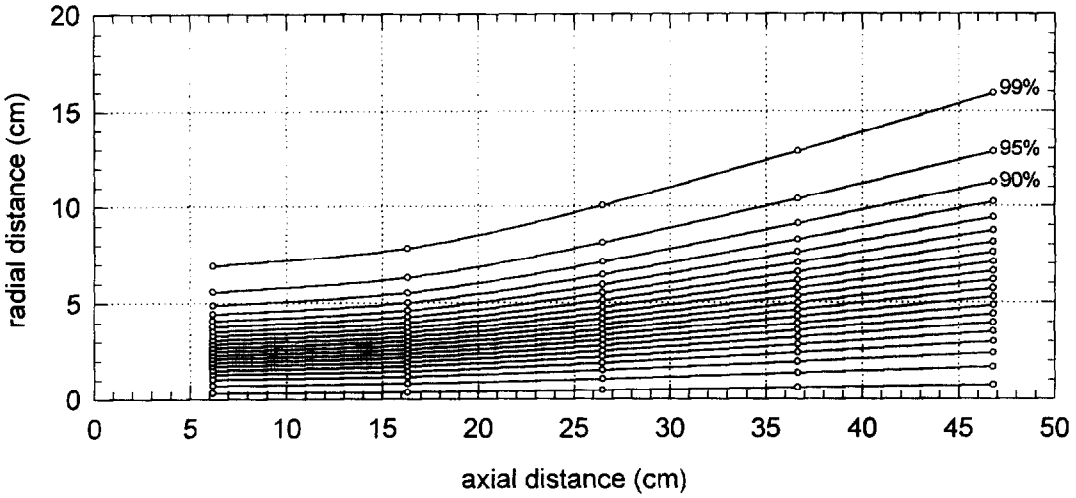

Figure 3. Integral flux contours for the data set in Fig. 2 enclose 1%, 5%, 10%, ... , 95%, and 99% of the total ion current.

can be obtained analytically. The Fourier and Hankel transforms of a Gaussian function are also Gaussians,[15,16] so that we have for the current density in polar coordinates,

$$\frac{d^2J}{r\,dr\,d\varphi} = \frac{J_{total}}{2\pi\sigma^2}\exp\left[-\frac{1}{2}\left(\frac{r}{\sigma}\right)^2\right], \qquad (6)$$

which, as expected, yields J_{total} when integrated over all r and φ. The radius enclosing a given fraction of the total beam current (say, 95%) is an implicit function of σ given by

$$\frac{1}{\sigma^2}\int_0^{r_{95}}\exp\left[-\frac{1}{2}\left(\frac{r}{\sigma}\right)^2\right] r\,dr = 0.95, \qquad (7)$$

which yields $r_{95} = 2.447747\ \sigma$.

The 95% flux contour is represented by graphing r_{95} vs. axial distance, as shown in Fig. 3 along with other contours from 1% to 99%. In the near-field region within 16 cm from the exit plane, the beam expands less rapidly than it does further downstream, as a consequence of the grids being dished inward. However, Fig. 3 for the 3-grid T5 at 18 mN nominal thrust does not show the well-developed beam waist that was observed at 15 cm axial distance in previous experiments using a short wire probe with a 2-grid T5 at 18 mN.[1] A possible explanation is a change in focusing properties due to the presence of the third grid or due to enlargement of the grid holes by erosion. Flux contours measured in 1987 for the 2-grid T5 at 10-mN display a waist 15-25 cm from the exit plane.[17]

Figures 4 and 5 show the 95% flux contour for 12 combinations of beam voltage (1000, 1100, 1200, 1300) and accelerator voltage (−150, −250, −350) at beam supply currents of 328 mA (nominal 18 mN at 1100 eV) and 457 mA (nominal 25 mN at 1100 eV). Figure 6 and 7 show the integrated beam current calculated using Eq. (2) for the same voltage combinations. When the accelerator grid is at −150 V, the integrated beam current is considerably less than the supply current, particularly at the higher beam voltages. This is indicative of electron backstreaming through the grid, accompanied by a sharp increase in the beam divergence. (A less eroded grid set would show less backstreaming than this one does at −150 V accelerator potential.) Across all the data sets, there is a decrease in the divergence as the beam voltage is made more positive. The other obvious trend is that the divergence is greater at 457 mA supply current than at 328 mA, as emphasized by the change in graph scales between Figs. 4 and 5. At 328 mA, an accelerator potential of −250 V gives a slightly higher beam current and a lower divergence than an accelerator potential of −350 V. At 457 mA these two potentials give approximately the same divergence and beam current.

The trends described here are summarized in Fig. 8 in terms of the 95% contour angle θ_{95}, which is taken to be the slope of the line drawn between the edge of the grid (x = 5 cm, z = 0) and r_{95} measured at the maximum distance from the exit plane ($x = r_{95}$, z = 46.8 cm). We showed in an earlier paper[3] that a rather incomplete picture of the high velocity ion flux is obtained by reducing the angular distribution to a single (arbitrarily defined) parameter such as θ_{95}, so the results in Fig. 8 should be used cautiously. The present values for θ_{95} are 2°- 4° smaller than the values measured previously for this grid set using a Faraday probe at 118 cm from the exit plane.[3] This is due in part to the greater sensitivity of the Faraday probe for fast ions at large angles (20° to 40° from centerline). It also indicates that the flux contours in Fig. 3 continue to curve outward further downstream, thus increasing the measured 95% contour angle.

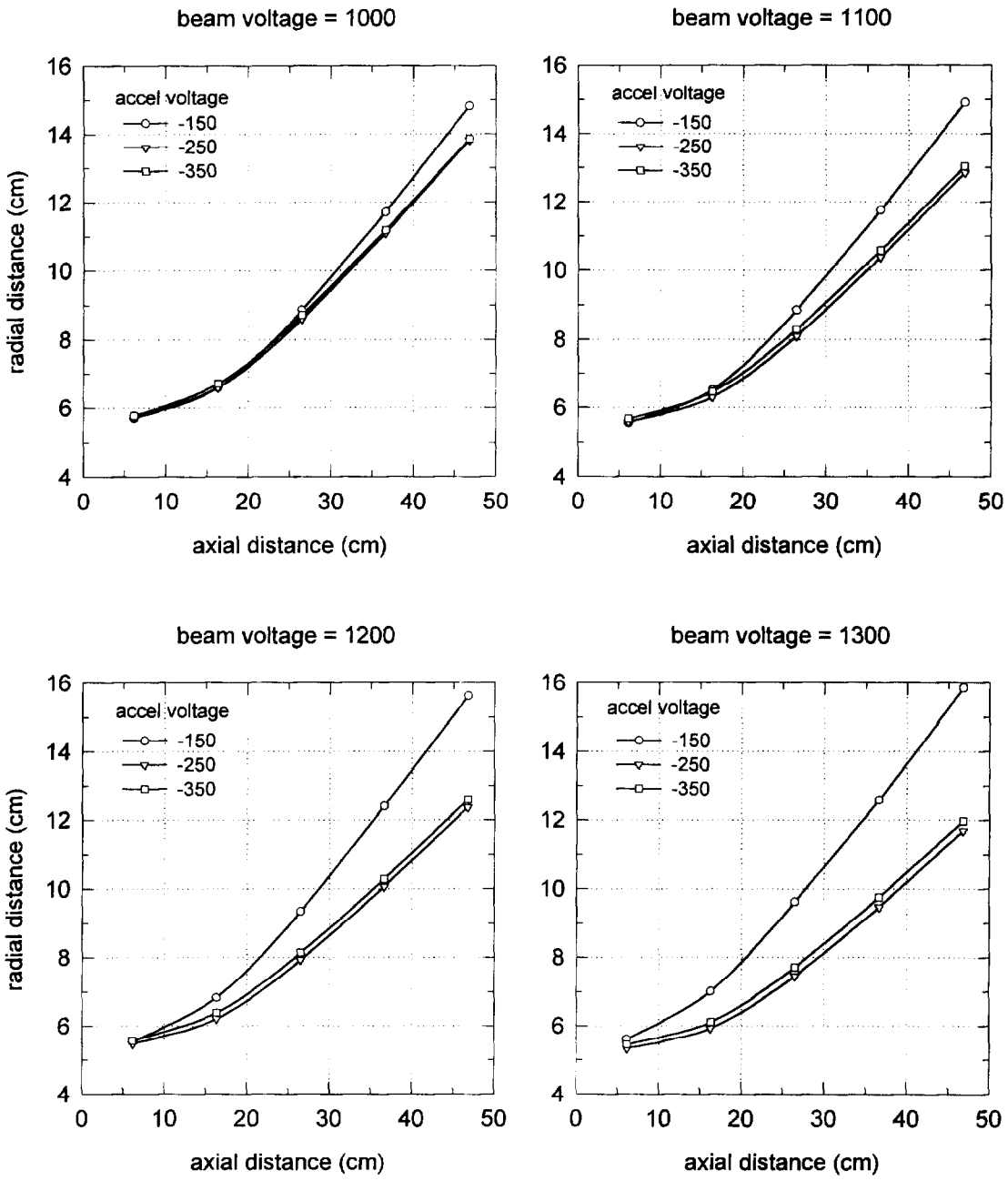

Figure 4. 95% flux contours at a supply current of 328 mA.

Previous investigations[18] of beam divergence for two- and three-grid ion accelerators provide guidance for interpreting the T5 results. Beamlet focusing is greatly affected by the position and curvature of the plasma sheath that forms upstream of each hole in the screen grid. For a given choice of grid potentials, there is an optimum plasma density that gives a sheath curvature corresponding to a minimum beam divergence. Increasing the beam current beyond this optimum point will increase the divergence, as happens in changing from 328 mA to 457 mA with the T5. Curvature of the neutralization surface downstream of each accelerator grid hole also tends to broaden the beamlet. This curvature decreases when the magnitude of the accelerator potential is reduced or the screen potential is increased, in agreement with most of our divergence data (neglecting the cases with −150 V on the accelerator). The presence of the decelerator grid makes this effect less important, but it still seems to be a factor with our eroded triple grid set.

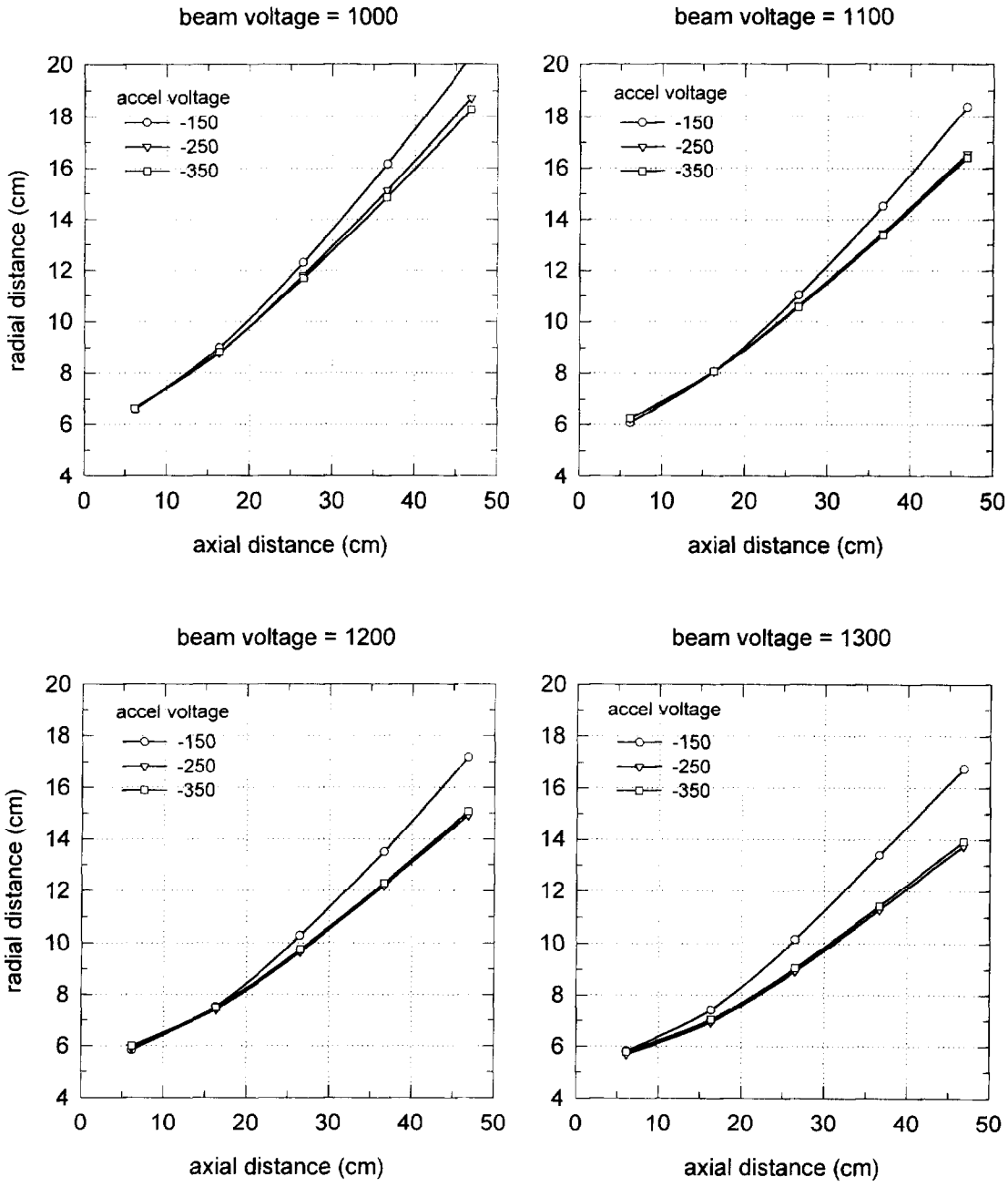

Figure 5. 95% flux contours at a supply current of 457 mA.

One observes in Figs. 6 and 7 a decrease in the integrated beam current with increasing axial distance, which is attributed to charge-exchange reactions with the background gas. Although there is no net loss of charge in the reaction Xe^{+}(fast) + Xe(slow) → Xe(fast) + Xe^{+}(slow), a depletion of the probe current is still expected because the slow Xe^{+} is accelerated away from the centerline by the plasma potential gradient.[1-3] For an estimated neutral gas density in the range of 0.5-1.0 × 10^{11} cm^{-3} and a path length of 40 cm, the observed depletion of 4%-7% corresponds to a phenomenological cross section of 1-3 × 10^{-14} cm^{2} or 100-300 $Å^{2}$. This is 3-8 times greater than the traditional value calculated from theory for Xe^{+1} + Xe charge exchange at 1100 eV.[19] The cross section for charge exchange reactions involving Xe^{+2} or metastable Xe^{+1} is likely be greater than that calculated for Xe^{+1} + Xe, which could partially explain the magnitude of our phenomenological cross section.

If the integrated beam currents in Fig. 6 are extrapolated back to the exit plane, the result equals the 328-mA supply current within 1% (neglecting the case

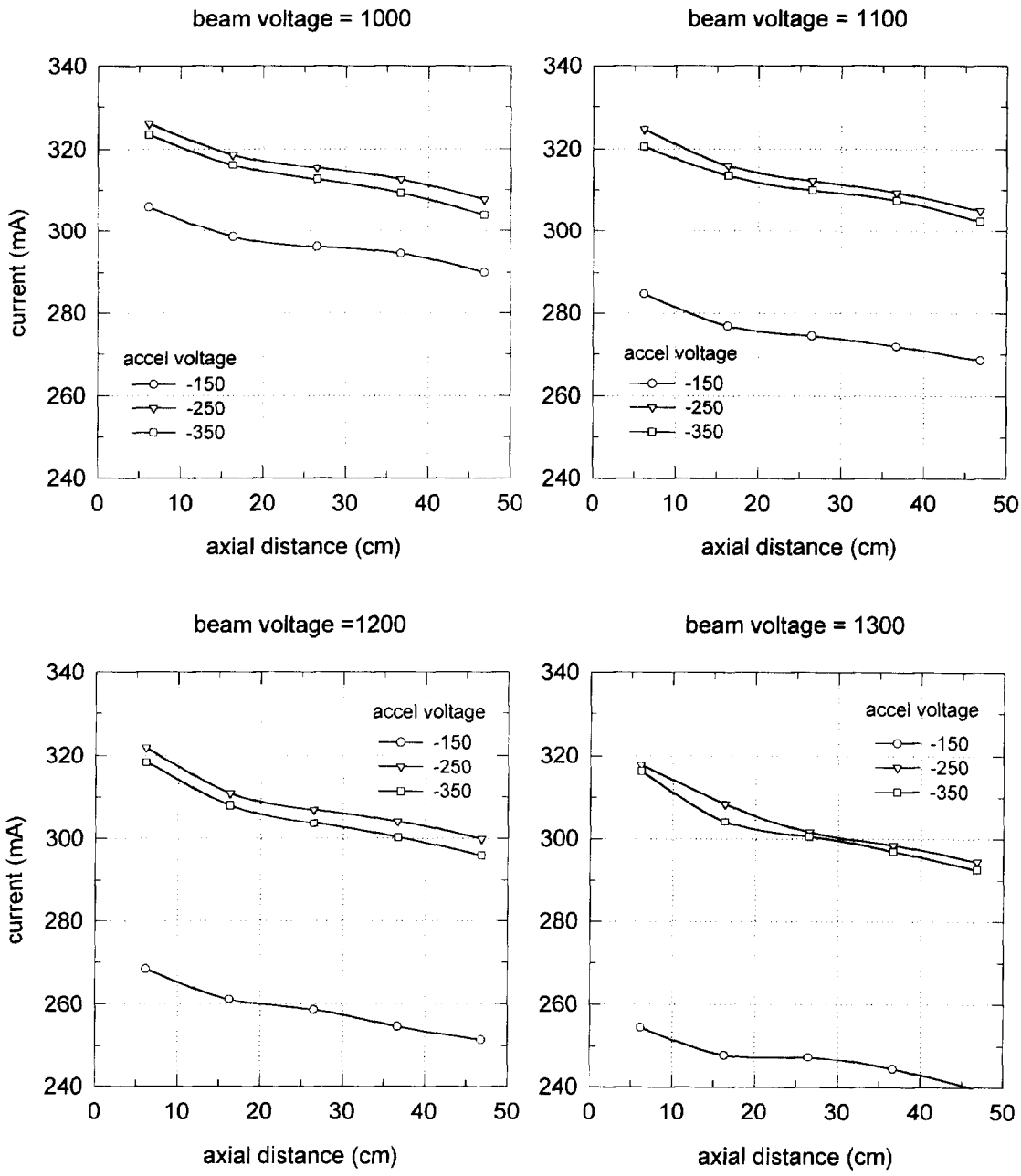

Figure 6. Integrated beam current at a supply current of 328 mA.

when the accelerator is −150 V). In Fig. 7 the integrated beam currents extrapolate to 440-450 mA, which is 2%-4% lower than the supply current of 457 mA. The discrepancy is attributed to leakage of electrons through the grids and plasma screen, which adds to the supply current but not to the beam current or thrust. The present observations corroborate our earlier thrust balance data[4] for which the difference between the directly measured thrust and the thrust calculated from the supply current grew larger as the thrust magnitude increased. Systematic error in the long wire probe experiment is no greater than ± 2% (arising from uncertainty in the wire diameter, secondary electron yield, and least-squares fitting). If the integrated beam currents in Figs. 6 and 7 are extrapolated out to 118 cm from the exit plane, the results are within 5% of the integrated beam currents obtained at 118 cm using an angle-resolving Faraday probe (265 mA and 378 mA).[3] Thus most of the difference between the supply current and the Faraday data is due to charge-exchange reactions with the background gas.

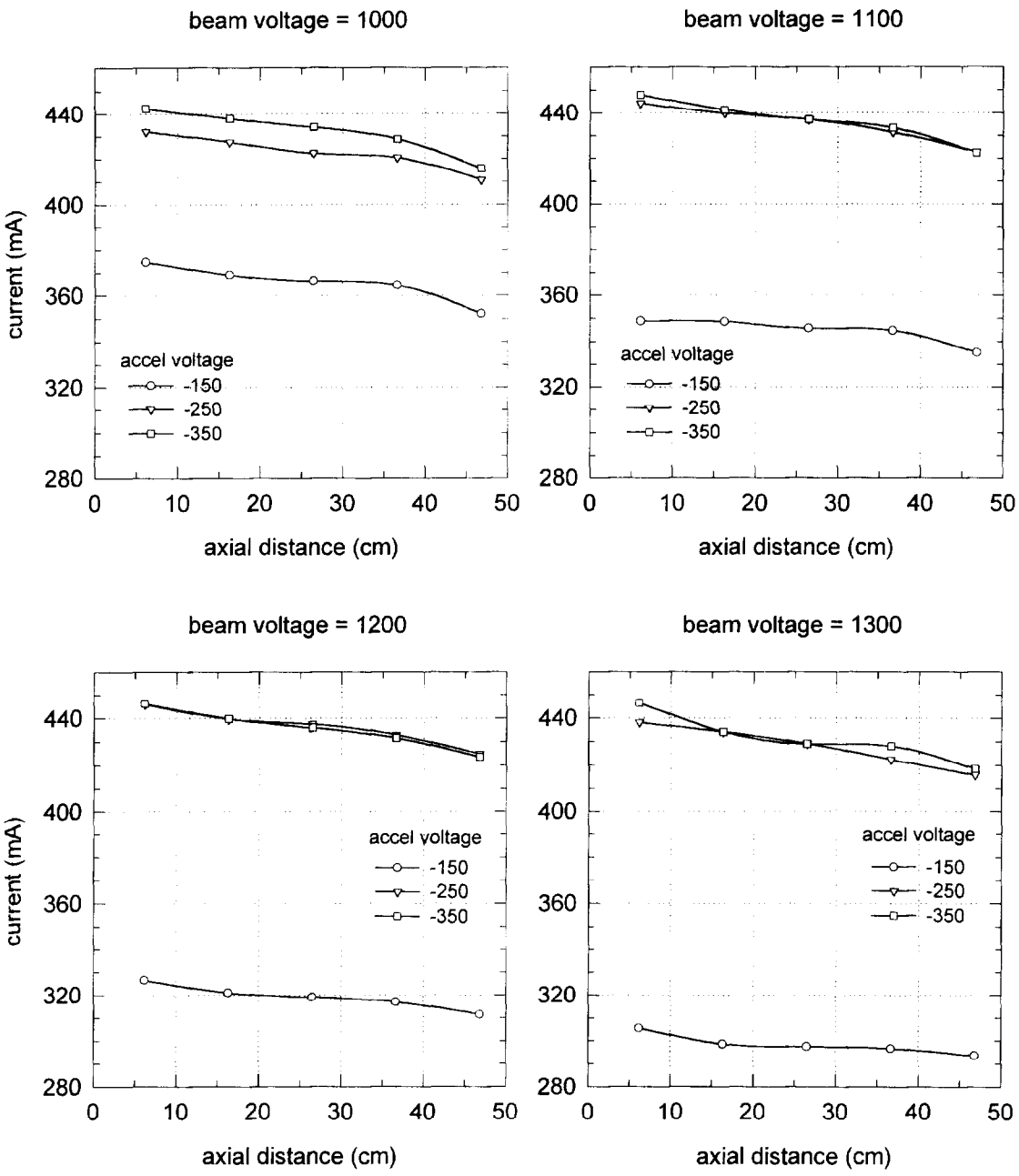

Figure 7. Integrated beam current at a supply current of 457 mA.

Acknowledgement

The author is grateful to P.C.T. de Boer, D.G. Fearn, and D.H. Mundy for providing valuable comments on interpreting the profile data. This work is supported by the Internal Research and Development Program at the Aerospace Corporation.

References

1. P.C.T. de Boer, "Electric probe measurements in the plume of an ion thruster," J. Propulsion and Power, 12, 95 (1996).

2. P.C.T. de Boer, "Measurements of electron density in the charge exchange plasma of an ion thruster," J. Propulsion and Power (in press).

3. J.E. Pollard, "Plume angular, energy, and mass spectral measurements with the T5 ion engine," Paper AIAA-95-2920, 31st Joint Propulsion Conference, 10-12 July 1995, San Diego, CA.

4. J.E. Pollard and R.P. Welle, "Thrust vector measurements with the T5 ion engine," Paper AIAA-95-2829, 31st Joint Propulsion Conference, 10-12 July 1995, San Diego, CA.

5. D.H. Mundy, "Factors affecting the beam divergence of a T5 ion engine," Paper IEPC-97-095, 25th International Electric Propulsion Conference, 24-28 Aug 1997, Cleveland, OH.

6. D.G. Fearn, A.R. Martin, and P. Smith, "Ion propulsion research and development in the UK," J. Brit. Interplan. Soc. 43, 431 (1990).

7. L.B. Loeb, Basic Processes of Gaseous Electronics, 2nd ed. (University of California Press, Berkeley, 1960), pp. 764-794 gives data for xenon ions on clean tungsten. Ejection of electrons from metal surfaces by the impact of xenon ions occurs mainly by an Auger-like process. The electron yield depends on the charge state of the ion and on the work function and surface coverage of the metal, but the yield is independent of the ion kinetic energy. We estimate that the electron yield is $\eta = 0.04$ for an ion beam containing 90% Xe^{+1} and 10% Xe^{+2}.

8. S.D. Watson, et al. "500 hour tests of the T5 ion thruster with dual and triple grid extraction systems," Paper IEPC-93-170, 23rd International Electric Propulsion Conference, 13-16 Sept 1993, Seattle, WA.

9. J.E. Pollard, "Beam -centroid tracking instrument for ion thrusters," Rev. Sci. Instrum. 65, 3733 (1994).

10. W.L. Barr, "Method for computing the radial distribution of emitters in a cylindrical source," J. Opt. Soc. Amer. 52, 885 (1962).

11. C.J. Cremers and R.C. Birkebak, "Application of the Abel integral equation to spectrographic data," Appl. Opt. 5, 1057 (1966).

12. M. Deutsch and I. Beniaminy, "Derivative-free inversion of Abel's integral equation," Appl. Phys. Lett. 41, 27 (1982).

13. E.W. Hansen and P.L. Law, "Recursive methods for computing the Abel transform and its inverse," J. Opt. Soc. Amer. 2, 510 (1985).

14. S.I. Sudharsanan, "The Abel inversion of noisy data using discrete integral transforms," M.S. Thesis, The University of Tennessee, Knoxville (Aug 1986).

15. E. Cavanagh and B.D. Cook, "Numerical evaluation of Hankel transforms via Gaussian-Laguerre polynomial expansions," IEEE Trans. Acous. Speech Sig. Proc. ASSP-27, 361 (1979).

16. S.M. Candel, "An algorithm for the Fourier-Bessel transform," Comp. Phys. Commun. 23, 343 (1981).

17. A.R. Martin, M.S. Harvey, and P.M. Latham, "Performance assessment of a UK rare gas ion thruster," Paper AIAA-87-1028, 19th International Electric Propulsion Conference, 11-13 May 1987, Colorado Springs, CO.

18. G. Aston, H.R. Kaufman, and P.J. Wilbur, "Ion beam divergence characteristics of two-grid accelerator systems," AIAA Journal, 16, 516 (1978); G. Aston and H.R. Kaufman, "Ion beam divergence characteristics of three-grid accelerator systems," AIAA Journal, 17, 64 (1979).

19. D. Rapp and W.E. Francis, "Charge exchange between gaseous ions and atoms," J. Chem. Phys. 37, 2631 (1962).

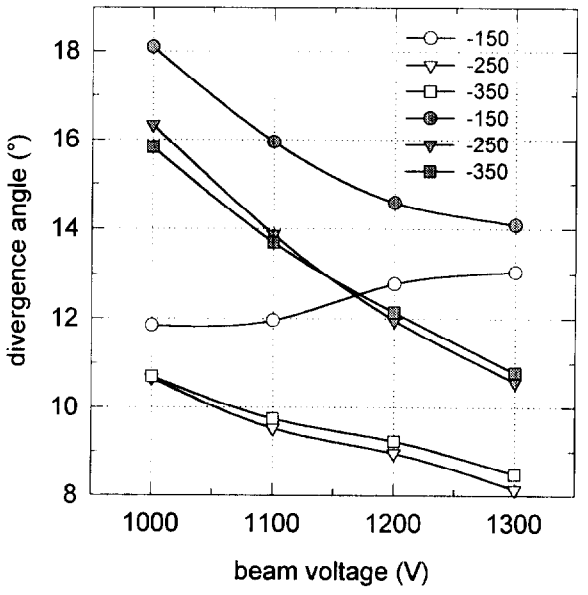

Figure 8. Divergence angle θ_{95} is calculated as the slope of the line connecting the grid edge (5-cm radius) with the radius enclosing 95% of the beam current at a downstream distance of 46.8 cm. Open symbols are for 328 mA supply current, and gray symbols are for 457 mA. Accelerator potential is −150, −250, and −350 V.